

Endocardium and Epicardium Segmentation in MR Images Based on Developed Otsu and Dynamic Programming

¹ Shengzhou XU, ² Chengdan PEI, ³* Huaifei HU

¹ College of computer science, South-Central University for Nationalities, Wuhan, 430074, China

² Wuhan Institute of Technology, Wuhan, 430074, China

³ College of biomedical engineering, South-Central University for Nationalities,
Wuhan, 430074, China

* E-mail: whkaociya@gmail.com

Received: 23 February 2014 / Accepted: 23 March 2014 / Published: 31 March 2014

Abstract: In order to accurately extract the endocardium and epicardium of the left ventricle from cardiac magnetic resonance (MR) images, a method based on developed Otsu and dynamic programming has been proposed. First, regions with high gray value are divided into several left ventricle candidate regions by the developed Otsu algorithm, which based on constraining the search range of the ideal segmentation threshold. Then, left ventricular blood pool is selected from the candidate regions and its convex hull is found out as the endocardium. The epicardium is derived by applying dynamic programming method to find a closed path with minimum local cost. The local cost function of the dynamic programming method consists of two factors: boundary gradient and shape features. In order to improve the accuracy of segmentation, a non-maxima gradient suppression technique is adopted to get the boundary gradient. The experimental result of 138 MR images show that the method proposed has high accuracy and robustness. *Copyright © 2014 IFSA Publishing, S. L.*

Keywords: Segmentation, Left ventricle, Endocardium, Epicardium, Dynamic programming, Otsu.

1. Introduction

Magnetic resonance (MR) image of the left ventricle (LV) is important for the diagnosis of a variety of cardiovascular diseases. And the segmentation of endocardium and epicardium is the key to the analysis and assessment of LV [1-2]. These segmentation methods can be classified into two generic categories: edge-based methods and region-based methods. The edge-based methods mainly include dynamic programming (DP) [3] and deformable models [4-5]. Due to the complexity of the myocardial contour, the classic DP algorithm is difficult to accurately extract the boundary;

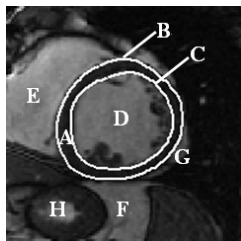
Deformable models include the snake model and level set [6-7], which susceptible to local minimum value, resulting in the evolution curves converge to the wrong surface of the heart wall. The region-based methods separate the region of interest from the background using the distribution of texture or gray level [8]. In MR image of the LV, due to the similar intensity distribution among myocardium, papillary muscle, liver, and chest wall, these methods may cause inaccurate results for LV segmentation. So, it is difficult to get an accurate outline of the LV use only one of edge-based methods or region-based methods. And, some hybrid segmentation methods combined with a variety of image

processing methods to obtain ventricular contours are presented [9].

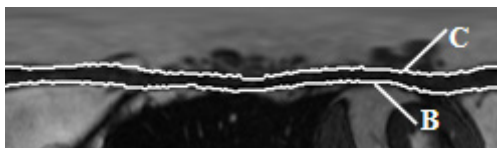
In this paper, a segmentation method combine with developed Otsu and dynamic programming is proposed to segment the endocardium and epicardium. First, a gray-scale restricted Otsu method is designed to segment LV blood pool, then, the convex hull of the blood pool is calculated as the endocardial contours. Based on this, take the MR image to be segmented as a cost graph, and the local cost function of each vertex composed of the shape factor and the gradient factor is constructed by taking full advantage of the characteristics of cardiac tissue. Then, the epicardial contour is obtained by looking for a path with least cost in the cost graph.

2. Endocardium Segmentation

Fig. 1 is the schematic diagram of LV in a region of interest (ROI) with a size of 101×101 pixels and its corresponding polar coordinate image. Region A is myocardial, contour line B and C are the epicardial and endocardial contours respectively, region D~H are LV blood pool, right ventricle blood pool, abdominal fat, pericardial fat and stomach respectively. The segmentation of endocardium and epicardium will be completed in the Cartesian coordinate image and the corresponding polar coordinate image respectively.



(a) the schematic diagram of LV in a ROI



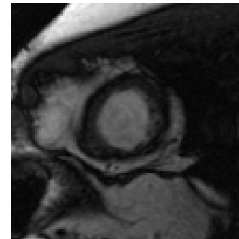
(b) Corresponding polar coordinate image

Fig. 1. Schematic diagram of the left ventricle and its corresponding polar coordinate image.

The Otsu threshold segmentation method is also known as the maximum margin criterion or the minimum sum of within-class variances criterion [10]. It becomes one of the most popular methods of threshold selection and has been widely applied because of the simple computation and well adaptation of maximum classes' square criterion which proposed in it. The Otsu method can achieve

good segmentation results when the difference between the gray level of the object and background is significant.

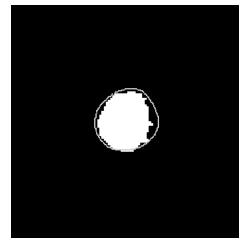
An important property of Otsu method has been discovered by the analysis of the properties of Otsu's threshold, which is that Otsu's threshold tends to be closer to the class with larger variance when the within-class variances of two classes are substantially different, which means that a part of pixels of this class will be classified into the other class [11].



(a) ROI to be segmented



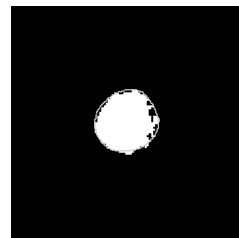
(b) Binary image obtained by Otsu method



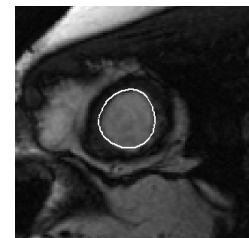
(c) Blood pool obtained by Otsu



(d) Binary image obtained by developed Otsu



(e) Blood pool obtained by developed Otsu



(f) Endocardium segmentation result

Fig. 2. Endocardium segmentation based on developed Otsu method.

Assume that a ROI image can be represented in L gray levels ($1, 2, \dots, L$). If it can be divided into two classes by a threshold at level T , i.e., the background represented by class C_1 consists of pixels of gray levels $[1, \dots, T]$ and the candidate target represented by class C_2 consists of pixels of gray levels $[T + 1, \dots, L]$. It can be known through experimentation and testing that the within-class variances of two classes are substantially different, and the background class C_1 have a lower variance.

Thus the LV blood pool is in the class C_2 and a part of pixels of this class has been classified into background class C_1 . It can within class C_1 (i.e., pixels lower than the threshold value T) again using the Otsu method to get a more accurate segmentation threshold. Based on the above analysis, an improved Otsu algorithm by constraining the search range of the ideal segmentation threshold has been proposed in this paper to segment the LV blood pool. The main steps are as follows.

- 1) Calculate the threshold T_1 by Otsu's method on the ROI image (as Fig. 2a), and the binary image can be obtained (as Fig. 2b).
- 2) Select the white area covering the center of ROI and remove the other white areas. Due to the Otsu threshold T_1 bias toward the candidate target class with larger variance, a part of pixels of the LV blood pool has been classified into the background class, as Fig. 2c. The white line is the gold standard of the edocardial contour.
- 3) Calculate the threshold T_2 by Otsu method in the pixels of the ROI image with gray level in $[1, T_1]$, and another binary image as shown in Fig. 2d can be obtained by applying the threshold T_2 on Fig. 2a.
- 4) Select the white area covering the center of ROI as the LV blood pool (shown as Fig. 2e), and remove the other white areas. Obviously, this area of blood pool is closer to the gold standard than the area in step 2.
- 5) Computing the convex hull of the blood pool area and using the fast Fourier transform to smooth the boundary, which as the result (shown as Fig. 2f) of the endocardial contour.

3. Epicardium Segmentation

The segmentation of epicardium is completed by dynamic programming method. To facilitate the calculation of cost function, the original ROI is transformed into polar ROI. The center of original ROI is selected to be the origin point (top left point) of the polar ROI. The radial line pointing horizontally from the center of the original ROI to the right is defined as the first column of the polar ROI, and the successive 359 radial lines anticlockwise are considered as the successive columns. So, the columns correspond to the angle θ from the horizontal and the rows correspond to the distance from the origin point. And $\theta = 0, 1, 2, \dots, 359$, $r = 0, 1, 2, \dots, 50$ (the maximum valid radius in ROI of size 101*101). A sample of the origin ROI and polar ROI are shown as Fig. 1. The epicardial contour, which is similar to a circle in the origin ROI, is close to a straight line in the polar ROI. After that, a cost graph can be constructed, where the pixels and the constraint relations between pixels of the polar ROI

are correspond to the vertices and the costs between vertices of the graph. The task of looking for the epicardial contour thereby is converted to searching a minimum cost path which is approximate a straight line. The minimum cost path optimization problems can be divided into two steps. In the first step, a local cost function which consists of boundary gradient and shape feature of the LV is constructed based on the characteristics of the epicardial contour. In the second phase, the epicardial contour is found by applying dynamic programming as an optimization technique.

3.1. Construction of Local Cost Function

Based on the above analysis, the local cost function C constructed in this study consists of the shape feature S and boundary gradient G :

$$C(r, \theta) = w_s S(r, \theta) + w_g G(r, \theta), \quad (1)$$

where parameters w_s, w_g are corresponding weights.

3.1.1. Boundary Gradient

The gradient of image is an important feature to reflect the presence or the strength of image edge. The larger the gradient value of a pixel, the more likely it is that an edge point of a region. Since the radial gradient of myocardial edge point more obvious, so the calculation of the radial gradient in polar coordinates is used as one factor of the cost function. Denoted the gray level of a pixel in the polar coordinate as $I(r, \theta)$, $1 \leq r \leq 50, 1 \leq \theta \leq 360$, then, the radial gradient of this pixel is calculated as follows.

$$\begin{aligned} & \text{if } 2 < r \leq 48 \\ & g(r, \theta) = |I(r+1, \theta) + I(r+2, \theta) - I(r-1, \theta) - I(r-2, \theta)| \\ & \text{else if } r \leq 2 \\ & g(r, \theta) = |I(r+1, \theta) - I(r, \theta)| \\ & \text{else} \\ & g(r, \theta) = |I(r, \theta) - I(r-1, \theta)| \end{aligned} \quad (2)$$

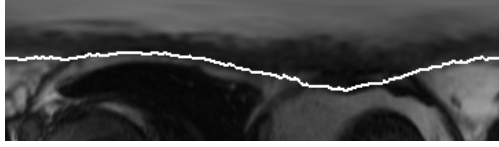
Then, the boundary gradient is calculated as the equation 3.

$$G(r, \theta) = \frac{g_{\max} - g(r, \theta)}{g_{\max}}, \quad (3)$$

where g_{\max} is the maximum radial gradient value of all candidate contour points.

The tissues surrounding myocardial are complex. There are right ventricular blood pool, abdominal fat,

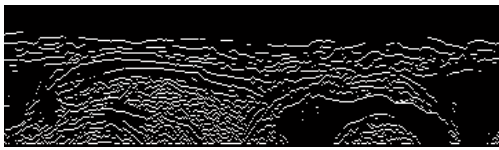
pericardial fat with high gray level and some other organizations with low gray level. The segmentation result might be interfered by these complex pixels with high gradient. As shown in Fig. 3a and b, the epicardial contour deviated from normal because of the attraction of the around pixels with high gradient.



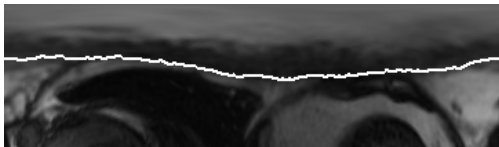
(a) Epicardial contour (polar coordinate) obtained by DP, not using non-maxima suppression



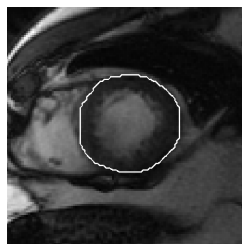
(b) Epicardial contour (Cartesian coordinate) obtained by DP, not using non-maxima suppression



(c) Non-maxima suppression gradient map



(d) Epicardial contour (polar coordinate) obtained by DP, using non-maxima suppression



(e) Epicardial contour (Cartesian coordinate) obtained by DP, using non-maxima suppression

Fig. 3. The non-maxima suppression strategy.

In order to avoid the confusing effect of the surrounding tissues, it needs to treat the weak edges (pixels with low gradient) of epicardium and strong edges of other organizations the same in boundary

gradient of local cost function, non-maxima suppression method is proposed to improve the calculation process of local cost. In the polar coordinate image's radial gradient matrix g , if $g(i, j) \geq g(i-1, j)$ and $g(i, j) \geq g(i+1, j)$, then the pixel at (i, j) is called local maxima of gradient. The local maxima points of the radial gradient image labeled 1, instead of maxima labeled 0, then, the non-maxima suppression gradient map can be obtained shown as in Fig. 3c. In this map, all local maxima pixels are given the same cost on boundary gradient, to avoid other organizations' pixels with high gradient to mislead the segmentation. In this study, the boundary gradient G of local cost function is constructed using the non-maxima suppression strategy and apply it to the dynamic programming algorithm to obtain the epicardial contour, the results are shown as Fig. 3d and 3e. Careful comparison of Fig. 3b and 3e, it can be found that the non-maxima suppression strategy can well prevent the interference from surrounding tissues and result in more accurate segmentation results.

3.1.2. Shape Feature

The shape factor of the local cost function is measured by the distance d through the current point to the next candidate. It is defined as follows.

$$S(r, \theta) = \begin{cases} \frac{d(r, \theta) - d_{\min}}{d_{\max} - d_{\min}} & \text{if } d(r, \theta) \leq dr \\ \infty & \text{else} \end{cases}, \quad (4)$$

where

$$d(r, \theta) = \sqrt{(r_{\theta} - r_{\theta-1})^2 + 1}, \quad (5)$$

r_{θ} and $r_{\theta-1}$ are the radiuses of the θ and $(\theta-1)$ columns respectively; d_{\max} and d_{\min} are the maximum and minimum distance between two candidate points of adjacent columns respectively. The parameter dr takes the value 3 in the experience, which is used to avoid drastic changes in the radius occurs between adjacent two columns, which may leading to an irregular shape of epicardial contour.

3.2. Dynamic Programming

After the construction of local cost function, the task of epicardial contour segmentation becomes a task to find the path with the smallest cumulative cost from the first to the last column in the polar coordinate image. In this paper, the dynamic programming algorithm is used to find the optimal path. The basic idea of dynamic programming

is breaking down the problem to be solved into several sub-problems, solving sub-problem first, and then get the solution of the original problem from the solution of these sub-problems. The cumulative cost of the dynamic programming algorithm is calculated by the following formula

$$\begin{aligned} & \text{if } (r < 3 \text{ or } r > 47) \text{ and } \theta \geq 0 \\ & CC(r, \theta + 1) = \infty \\ & \text{else if } (3 \leq r \leq 47) \text{ and } \theta = 0 \\ & CC(r, \theta + 1) = C(r, 0) \\ & \text{else} \\ & CC(r, \theta + 1) = \min_{-3 \leq l \leq 3} CC(r - l, \theta) + C(r, \theta + 1), \end{aligned} \quad (6)$$

where C is the local cost function, CC is the cumulative cost, l represents the direction of movement from column θ to column $\theta + 1$. In the initial state, the search starts from the points on the first column, and the distance value r of each column is defined within the range of 3 to 47. The cumulative cost value of the starting point is equal to its local cost value $C(r, 0)$.

Each candidate point of epicardial contour on the first column corresponds to a series of candidate path which constituted by 360 points (one point for each column). In order to ensure the path which represent epicardial contour is closed, the end points of these paths are designed back to the corresponding start points on the first column. The path with the minimum cumulative cost will be selected as the best path, the pixels on which are connected to form a continuous contour as the epicardial contour.

4. Experimental Results and Analysis

Fig. 4 shows the segmentation results using the method proposed in this paper on 12 randomly selected ROI image. As can be seen from the figure: for endocardial contour segmentation, the gray-scale restricted Otsu method is able to get a reasonable threshold, and the fast Fourier transform makes a very smooth boundary; for epicardial contour, the local cost function of dynamic programming method fully considers the morphological and gray characteristics, so that the method can eliminate the influence of the complexity surrounding tissue on the segmentation results, making the segmentation result is not compromised.

In order to quantitatively analyze the difference between the segmentation results of the method proposed in this paper and the gold standards (radiologists' manual segmentation result), the areas overlap measure AOM and the average minimum Euclidean distance AMED are used to measure the closeness between the segmentation results and the gold standards. AOM is defined as the ratio between

the intersection and union sets of the segmentation result and gold standard.

$$AOM = \frac{A_{seg} \cap A_{gs}}{A_{seg} \cup A_{gs}}, \quad (7)$$

where A_{seg} represents the target region obtained by the segmentation method, and A_{gs} represents the gold standard obtained by radiologists' manual segmentation. The value of AOM can reflect the degree of overlap between segmentation result and gold standard.

The value of AMED can accurately reflect the closeness of the contours of segmentation results and gold standards. Assuming the contour of segmentation result is $A = \{a_1, a_2, \dots, a_m\}$, and the contour of gold standard is $B = \{b_1, b_2, \dots, b_n\}$, the value of AMED is calculated as follows.

$$AMED(A, B) = \left(\frac{1}{m} \sum_{i=1}^m d(a_i, B), \frac{1}{n} \sum_{j=1}^n d(b_j, A) \right) / 2, \quad (8)$$

where $d(a_i, B)$ is the minimum distance of point a_i to all the points on contour B . Therefore, $AMED(A, B)$ reflects the overall distribution of the distance between corresponding point on the boundaries A and B .

In order to verify the effectiveness of the algorithm proposed in this paper, the segmentation results of our method, Lu's method [8] and Huang's method [9] are compared on 138 images. The AOM and AMED values of the segmentation results of above three algorithms are shown in Table 1.

Table 1. Comparison of segmentation results.

Method	AOM (%)		AMED (mm)	
	endo-	epi-	endo-	epi-
Ours	0.89	0.92	1.86	2.02
Lu's	0.86	0.88	2.13	2.32
Huang's	0.85	0.89	2.24	2.29

Obviously, the AOM value of our method is significantly higher than the other two algorithms, that's to say the areas surrounded by the endocardial and epicardial contours obtained by our method are closer to the areas surrounded by the gold standards. On the other hand, the AMED value of our method is significantly smaller than the other two methods, this shows that the contours obtained by our method are closer to the gold standard contours. Therefore, our method has a good performance on endocardial and epicardial contour segmentation (Fig. 4).

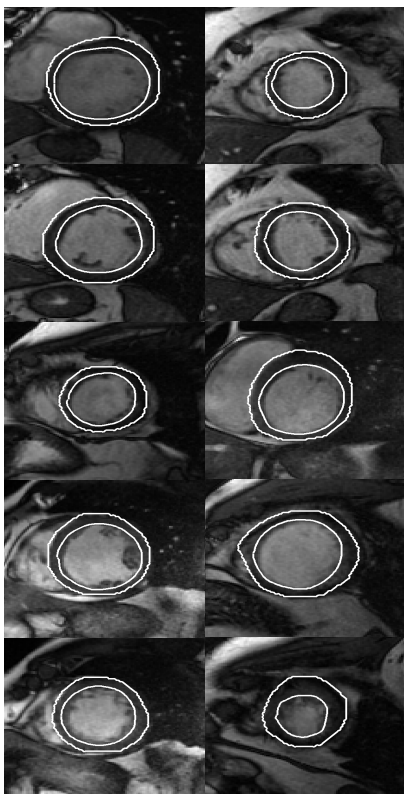


Fig. 4. Endocardium and epicardium segmentation results.

5. Conclusions

An automatic segmentation method based on improved Otsu method and dynamic programming has been proposed to get the endocardium and epicardium in this paper. The endocardium is segmented by finding and smoothing the convex hull of the LV blood pool, which is obtained by the developed Otsu algorithm. The developed Otsu gets accurate threshold by constraining the search range of the ideal segmentation threshold; Epicardium segmentation using a dynamic programming method with non-maxima suppression, which not only make use of the gradient and morphological information, and can prevent the epicardial contour deviated from normal because of the attraction of the around pixels with high gradient.

Acknowledgements

This work was supported in part by the National Natural Science Foundation of China (No. 61302192), the Fundamental Research Funds for the Central Universities (No.CZQ13010).

References

- [1]. C. Nambakhsh, J. Yuan, K. Punithakumar, et al., Left Ventricle Segmentation in MRI via Convex Relaxed Distribution Matching, *Medical Image Analysis*, Vol. 17, Issue 8, 2013, pp. 1010-1024.
- [2]. A. Eslami, A. Karamalis, A. Katouzian, et al., Segmentation by retrieval with guided random walks: Application to left ventricle segmentation in MRI, *Medical Image Analysis*, Vol. 17, Issue 2, 2013, pp. 236-253.
- [3]. Uzümcü M., van der Geest R. J., Swingen C., Reiber J. H., Lelieveldt B.P., et al., Time continuous tracking and segmentation of cardiovascular magnetic resonance images using multidimensional dynamic programming, *Investigative Radiology*, Vol. 41, Issue 1, 2006, pp. 52-62.
- [4]. T. Chen, J. Babb, P. Kellman, et al., Semiautomated segmentation of myocardial contours for fast strain analysis in cine displacement-encoded MRI, *IEEE Transactions on Medical Imaging*, Vol. 27, Issue 8, 2008, pp. 1084-1094.
- [5]. L. Hae, N. C. F. Codella, M. D. Cham, et al., Automatic Left Ventricle Segmentation Using Iterative Thresholding and an Active Contour Model With Adaptation on Short-Axis Cardiac MRI, *IEEE Transactions on Biomedical Engineering*, Vol. 57, Issue 4, 2010, pp. 905-913.
- [6]. N. Zhang, X. Yu, G. Lu, Endocardium and epicardium segmentation of left ventricle in cardiac magnetic resonance images based on directional Snake model, *Journal of Computer Applications*, Vol. 32, Issue 7, 2012, pp. 1902-1905.
- [7]. G. Wang, J. Zhang, Y. Chen, et al., An Anisotropic GVF Model for the MR Image Segmentation of Left Ventricle, *Journal of Computer-Aided Design & Computer Graphics*, Vol. 22, Issue 11, 2010, pp. 1887-1891.
- [8]. Y. Lu, P. Radau, K. Connelly, et al., Segmentation of left ventricle in cardiac cine MRI: An automatic image-driven method, in *Lecture Notes in Computer Science*, Vol. 5528, 2009, pp. 339-347.
- [9]. S. Huang, J. Liu, L. Lee, et al., An image-based comprehensive approach for automatic segmentation of left ventricle from cardiac short axis cine mr images, *Journal of Digital Imaging*, Vol. 24, Issue 4, 2011, pp. 598-608.
- [10]. Y. Xu, J. Tian, C. Wang, et al., Infrared mountain detection based on nested Otsu segmentation and contour extraction, *Journal of Computer Applications*, Vol. 33, Issue S1, 2013, pp. 199-200.
- [11]. X. Xu, S. Xu, L. Jin, et al. Characteristic analysis of Otsu threshold and its applications, *Pattern Recognition Letters*, Vol. 32, Issue 7, 2011, pp. 956-961.